

# Journal of Biomedical Optics

BiomedicalOptics.SPIEDigitalLibrary.org

## **Algorithm for removing scalp signals from functional near-infrared spectroscopy signals in real time using multidistance optodes**

Masashi Kiguchi  
Tsukasa Funane

# Algorithm for removing scalp signals from functional near-infrared spectroscopy signals in real time using multidistance optodes

Masashi Kiguchi\* and Tsukasa Funane

Hitachi Ltd., Central Research Laboratory, Hatoyama, Saitama 350-0395, Japan

**Abstract.** A real-time algorithm for removing scalp-blood signals from functional near-infrared spectroscopy signals is proposed. Scalp and deep signals have different dependencies on the source-detector distance. These signals were separated using this characteristic. The algorithm was validated through an experiment using a dynamic phantom in which shallow and deep absorptions were independently changed. The algorithm for measurement of oxygenated and deoxygenated hemoglobins using two wavelengths was explicitly obtained. This algorithm is potentially useful for real-time systems, e.g., brain-computer interfaces and neuro-feedback systems. © The Authors. Published by SPIE under a Creative Commons Attribution 3.0 Unported License. Distribution or reproduction of this work in whole or in part requires full attribution of the original publication, including its DOI. [DOI: 10.1117/1.JBO.19.11.110505]

Keywords: infrared imaging; biomedical optics; scalp blood flow.

Paper 140524LRR received Aug. 19, 2014; accepted for publication Oct. 29, 2014; published online Dec. 1, 2014.

## 1 Introduction

Functional near-infrared spectroscopy (fNIRS)<sup>1</sup> has been used for observing brain activity in the fields that require everyday measurements because the equipment is smaller, more inexpensive, and requires less restriction of subjects than other neuro-imaging modalities such as functional MRI and PET. Since the light is irradiated and detected from the brain through the scalp, the effects of hemodynamic changes in the scalp on the fNIRS signals have been reported.<sup>2,3</sup> Therefore, an experimental design that compensates these effects using adequate control conditions is required.

To lift or relax this limitation, several engineering techniques have been developed.<sup>4-6</sup> The multidistance independent analysis (MD-ICA) method using multidistance optodes<sup>7</sup> has an advantage in that scalp signals can be quantitatively separated from the obtained signals. However, the real-time process of MD-ICA has not been achieved due to ICA, which requires time series data, although some other techniques are applicable for real-time processing. Because the scalp-signal effect potentially changes during experiments due to changes in emotion, the real-time separation is helpful to determine whether to stop or

redo the experiment to increase measurement throughput. The real-time separation is also required for the brain-computer interface and neuro-feedback systems that have been applied in rehabilitation. We modified the algorithm of MD-ICA for real-time processing and validated the algorithm through an experiment using a dynamic phantom.

## 2 Method

The absorbance change  $\Delta A$  is proportional to the sum of the product of change in hemoglobin concentration  $c_i$  and partial path length  $l_i$  in region  $i$  according to the modified Beer-Lambert equation in the case where the changes in partial path lengths are negligible

$$\Delta A = \sum_i (\epsilon \Delta c_i l_i) \equiv \epsilon (\Delta c l), \quad (1)$$

where  $\epsilon$  is the molecular extinction coefficient for hemoglobin. Since the continuous-wave fNIRS (cw-fNIRS) cannot separately measure  $c_i$  and  $l_i$ , the effective values of  $c$  and  $l$  are defined when the hemoglobin concentration changes in the scalp and the deep tissue

$$\Delta A = \epsilon (\Delta c l)_{\text{deep}} + \epsilon (\Delta c l)_{\text{scalp}}. \quad (2)$$

The dependency of the partial path length on the source-detector (SD) distance  $d$  has been calculated using a slab model<sup>7</sup> and the real-head anatomical model obtained through MRI.<sup>8</sup> The partial path length in scalp is approximately constant when  $d$  is larger than about 10 mm. The partial path length in the deep tissue linearly increases when  $d$  is larger than  $d_0$ .

$$l_{\text{deep}} = l_0 \cdot (d/d_0 - 1). \quad (3)$$

Here,  $d_0$  and  $l_0$  are the  $x$ -intercept and the minus value of  $y$ -intercept, respectively, when the partial path length in the deep tissue is plotted to  $d$ .

In MD-ICA, independent components were calculated by time-delayed decorrelation ICA (TDD-ICA) using absorbance changes observed with multiple values of  $d$ , then each weight factor for each independent component was divided into a deep subcomponent and a scalp subcomponent according to the ratio of the partial path length for deep tissue and scalp calculated using the  $d$  dependency of signal intensity. The deep and scalp components were reconstructed using all deep subcomponents and scalp subcomponents, respectively. The TDD algorithm requires a certain time period of measured absorbance changes, usually the period of a measurement cycle. Therefore, MD-ICA was used in the postprocess.

The MD-ICA algorithm can be easily modified for real-time processing by removing the ICA process. We call the new algorithm the real-time scalp signal separating (RT-SSS) algorithm. In MD-ICA, the separation process was applied to each independent component obtained by ICA. In RT-SSS, the separation process was applied not to the independent component, but directly to the absorbance change. The absorbance change observed with SD distance  $d$ ,  $\Delta A[d, t]$  can be separated into those for the deep and scalp layers,  $\Delta A_{\text{deep}}^{\text{RT-SSS}}[d, t]$  and  $\Delta A_{\text{scalp}}^{\text{RT-SSS}}[d, t]$  using Eqs. (2) and (3).

$$\Delta A[d, t] = \Delta A_{\text{deep}}^{\text{RT-SSS}}[d, t] + \Delta A_{\text{scalp}}^{\text{RT-SSS}}[d, t], \quad (4)$$

$$\Delta A_{\text{deep}}^{\text{RT-SSS}}[d, t] = \epsilon \cdot (\Delta c l_0)_{\text{deep}}[t] \cdot (d/d_0 - 1), \quad (5)$$

\*Address all correspondence to: Masashi Kiguchi, E-mail: [masashi.kiguchi.py@hitachi.com](mailto:masashi.kiguchi.py@hitachi.com)

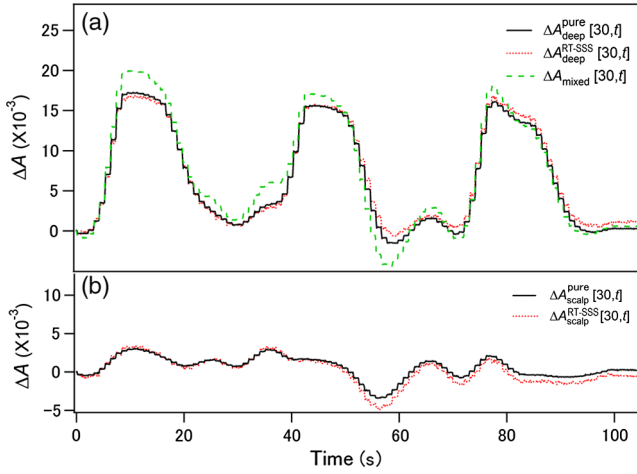


**Fig. 1** (a) Time series of deep absorbance change obtained using RT-SSS algorithm, mixed absorbance change, and pure deep absorbance change. (b) Time series of scalp absorbance change obtained using RT-SSS algorithm and pure scalp absorbance change.

$$\Delta A_{\text{scalp}}^{\text{RT-SSS}}[d, t] = \varepsilon \cdot (\Delta c l)_{\text{scalp}}[t]. \quad (6)$$

The  $\Delta A_{\text{deep}}^{\text{RT-SSS}}[d_1, t]$  and  $\Delta A_{\text{scalp}}^{\text{RT-SSS}}[d_1, t]$  can be calculated for each time  $t$  from  $\Delta A[d_1, t]$  and  $\Delta A[d_2, t]$  observed with different two values of  $d$ ,  $d_1$  and  $d_2$ , when  $d_0$  is given as well as MD-ICA. The parameters  $\Delta(c l)_{\text{deep}}$  and  $\Delta(c l)_{\text{scalp}}$  are effective ones for the two homogeneous layer models. The deviation of  $d_0$  caused by the inhomogeneity in the depth direction leads to the cross talk between the separated signals of scalp and deep regions. The errors of separation were investigated in the previous paper for MD-ICA.<sup>7</sup> Although two values of  $d$  are required for solving equations, using more than three values of  $d$  potentially reduces the error of separation due to the lateral inhomogeneity of absorbance in the scalp caused by the inhomogeneous distribution of scalp veins.

In RT-SSS, the noise is artificially divided into scalp and deep components depending on its SD-distance dependency.

Each noise included in scalp or deep signals can be reduced by the usual algorithms of noise reduction in the postprocess.

### 3 Experimental Validation Using a Dynamic Phantom

The RT-SSS algorithm was validated using a dynamic phantom.<sup>9</sup> The dynamic phantom had two (upper and lower) scattering and absorbing layers, and the absorption changes in the two layers were independently created by their motions driven by two moving stages. We measured the absorbance changes by using the phantom irradiated by a diode-laser light with a wavelength of 695 nm at  $d = 15$  and 30 mm under three conditions: (1) only the absorption of the lower layer was changed with a specified activation pattern, (2) only the absorption of the upper layer was changed with another activation pattern, and (3) the absorptions of both the lower and upper layers were changed with the activation patterns used for the conditions 1 and 2, respectively.

When considering that  $d = 30$  mm is commonly employed in fNIRS, the absorbance change measured at  $d = 30$  mm under condition 1 was the pure signal originating from the deep (lower) layer. The absorbance change measured at  $d = 30$  mm under condition 2 was the pure signal originating from the scalp (upper) layer. The absorbance change measured at  $d = 30$  mm under condition 3 was the mixed signal originating from both the deep and scalp layers. These three absorbance changes are expressed as  $\Delta A_{\text{deep}}^{\text{pure}}$ ,  $\Delta A_{\text{scalp}}^{\text{pure}}$ , and  $\Delta A_{\text{mixed}}$ , respectively. The absorbance changes in the deep and scalp layers obtained using the RT-SSS algorithm with  $\Delta A_{\text{mixed}}[15, t]$  and  $\Delta A_{\text{mixed}}[30, t]$  are also expressed as  $\Delta A_{\text{deep}}^{\text{RT-SSS}}$  and  $\Delta A_{\text{scalp}}^{\text{RT-SSS}}$ , respectively.

The value of  $d_0$  for the phantom required the use of Eq. (5). It was experimentally measured as follows. Under condition 1,  $\Delta A_{\text{deep}}^{\text{RT-SSS}}$  of Eq. (5) can be replaced by  $\Delta A_{\text{deep}}^{\text{pure}}$ . Then, we can write the following equation:

$$\frac{\Delta A_{\text{deep}}^{\text{pure}}[30, t]}{\Delta A_{\text{deep}}^{\text{pure}}[15, t]} = \frac{30 - d_0}{15 - d_0}. \quad (7)$$

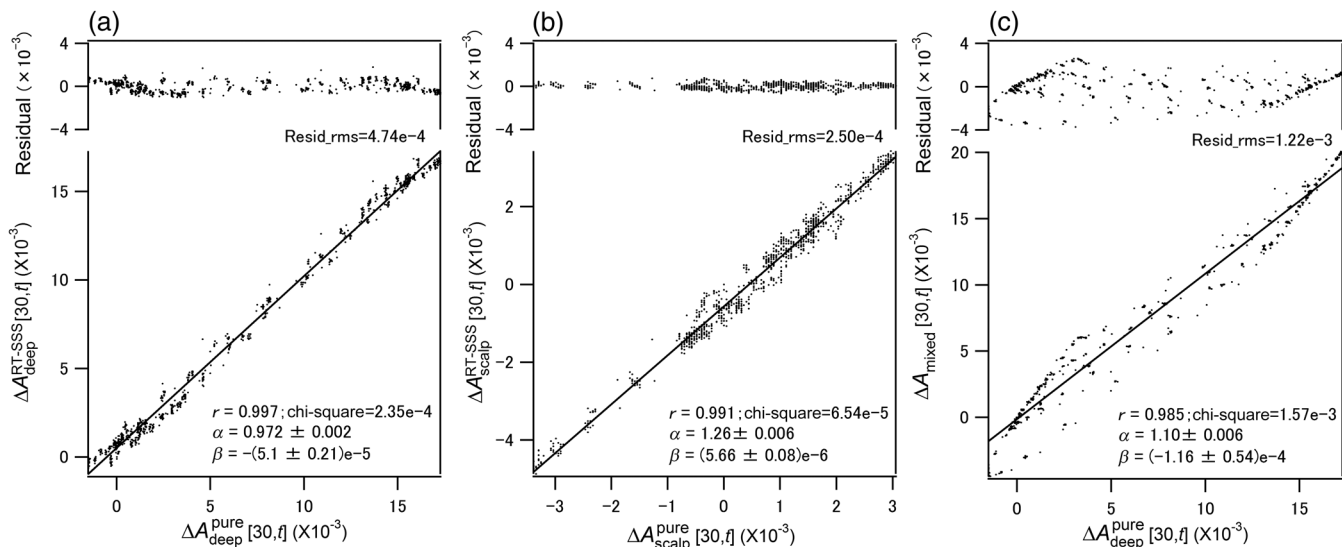


**Fig. 2** Correlation between (a) deep absorbance change separated using RT-SSS algorithm, (b) scalp absorbance change separated using RT-SSS algorithm, (c) mixed absorbance change and respective pure absorbance change.

By the least square fitting with Eq. (7),  $d_0$  was obtained as 9.92 mm. Note that these values  $d_0$  change depending on the characteristics of the phantom, i.e., materials, structure, and so on.

The mixed absorbance change measured with  $d = 30$  mm,  $\Delta A_{\text{mixed}}[30, t]$  and the separated deep and scalp absorbance changes using the RT-SSS algorithm,  $\Delta A_{\text{deep}}^{\text{RT-SSS}}[30, t]$  and  $\Delta A_{\text{scalp}}^{\text{RT-SSS}}[30, t]$  are compared with the pure absorbance changes  $\Delta A_{\text{deep}}^{\text{pure}}[30, t]$  and  $\Delta A_{\text{scalp}}^{\text{pure}}[30, t]$  in Fig. 1. Each absorbance change separated using the RT-SSS algorithm agreed with each pure absorbance change for both deep and scalp tissues. Figure 2 shows the correlation between (a) the deep absorbance change, (b) scalp absorbance change and each corresponding pure absorbance change, and (c) the mixed absorbance change and pure deep absorbance change. The fitting coefficients, slope  $\alpha$  and y-intercept  $\beta$ , are shown in Fig. 2. The correlation coefficients  $r$  between the RT-SSS absorbance change and pure

absorbance change for deep tissue and scalp were 0.997 and 0.991, respectively. The chi-squares were small enough and the residual waveform was flat. For the mixed absorbance change, however, the correlation coefficient was smaller, the chi-square was larger, and the residual waveform was more distorted than those for RT-SSS absorbance change because the mixed absorbance change includes both deep and scalp ones. Therefore, we can conclude that the RT-SSS algorithm successfully separated the mixed absorbance change into deep and scalp absorbance changes.

## 4 Discussions and Conclusions

The RT-SSS algorithm was explicitly applied to oxygenated and deoxygenated hemoglobin measurements using two wavelengths. From Eqs. (4) to (6), each absorbance change at wavelengths  $\lambda_1$  and  $\lambda_2$  measured with  $d_1$  and  $d_2$  was written as

$$\begin{pmatrix} \Delta A^{\lambda_1}[d_1, t] & \Delta A^{\lambda_1}[d_2, t] \\ \Delta A^{\lambda_2}[d_1, t] & \Delta A^{\lambda_2}[d_2, t] \end{pmatrix} = \begin{pmatrix} \varepsilon_{\text{oxy}}^{\lambda_1} & \varepsilon_{\text{deoxy}}^{\lambda_1} \\ \varepsilon_{\text{oxy}}^{\lambda_2} & \varepsilon_{\text{deoxy}}^{\lambda_2} \end{pmatrix} \times \begin{pmatrix} (\Delta c_{\text{oxy}} l)_{\text{deep}}[d_1, t] + (\Delta c_{\text{oxy}} l)_{\text{scalp}}[d_1, t] & (\Delta c_{\text{oxy}} l)_{\text{deep}}[d_2, t] + (\Delta c_{\text{oxy}} l)_{\text{scalp}}[d_2, t] \\ (\Delta c_{\text{deoxy}} l)_{\text{deep}}[d_1, t] + (\Delta c_{\text{deoxy}} l)_{\text{scalp}}[d_1, t] & (\Delta c_{\text{deoxy}} l)_{\text{deep}}[d_2, t] + (\Delta c_{\text{deoxy}} l)_{\text{scalp}}[d_2, t] \end{pmatrix}, \quad (8)$$

with

$$(\Delta c_{\text{oxy}} l)_{\text{deep}}[d, t] = (\Delta c_{\text{oxy}} l_0)_{\text{deep}}[t] \cdot (d/d_0 - 1), \quad (9)$$

$$(\Delta c_{\text{deoxy}} l)_{\text{deep}}[d, t] = (\Delta c_{\text{deoxy}} l_0)_{\text{deep}}[t] \cdot (d/d_0 - 1), \quad (10)$$

$$(\Delta c_{\text{oxy}} l)_{\text{scalp}}[d_1, t] = (\Delta c_{\text{oxy}} l)_{\text{scalp}}[d_2, t], \quad (11)$$

$$(\Delta c_{\text{deoxy}} l)_{\text{scalp}}[d_1, t] = (\Delta c_{\text{deoxy}} l)_{\text{scalp}}[d_2, t], \quad (12)$$

where  $\varepsilon_{\text{oxy}}^{\lambda}$  and  $\varepsilon_{\text{deoxy}}^{\lambda}$  represent the molecular extinction coefficient at wavelength  $\lambda$  for oxygenated and deoxygenated hemoglobins, respectively. Also  $\Delta c_{\text{oxy}}$  and  $\Delta c_{\text{deoxy}}$  are the change in concentration of oxygenated and deoxygenated hemoglobins, respectively. Here,  $d_0$  was assumed to be independent of the wavelength in the case of human measurement. When  $d_0$  and  $\varepsilon$  are given, the deep and scalp hemoglobin signals are separated by solving Eq. (8) for four unknowns of  $(\Delta c_{\text{oxy}} l)_{\text{deep}}[d, t]$ ,  $(\Delta c_{\text{deoxy}} l)_{\text{deep}}[d, t]$ ,  $(\Delta c_{\text{oxy}} l)_{\text{scalp}}[d, t]$  and  $(\Delta c_{\text{deoxy}} l)_{\text{scalp}}[d, t]$  since the elements of the matrix on the left-hand side of Eq. (8) are directly measurable at each time,  $t$ . The literature values of  $\varepsilon$  for hemoglobin can be used. The value of  $d_0$  for the human forehead was estimated to be  $10.5 \pm 1.6$  mm by stanching the scalp blood flow, and the errors in the calculated hemoglobin caused by the variation in the value of  $d_0$  were also estimated in the previous paper on MD-ICA.<sup>7</sup> Because the concept of RT-SSS is almost the same as that of MD-ICA, the effect of the variation of  $d_0$  must also be almost the same.

In conclusion, we proposed the RT-SSS algorithm using two  $d$  measurements and validated it through phantom experiments. This algorithm will be applied to human experiments to verify its effectiveness.

## References

1. F. Scholkmann et al., "A review on continuous wave functional near-infrared spectroscopy and imaging instrumentation and methodology," *Neuroimage* **85**, 6–27 (2014).
2. P. Smielewski et al., "Clinical evaluation of near-infrared spectroscopy for testing cerebrovascular reactivity in patients with carotid artery disease," *Stroke* **28**, 331–338 (1997).
3. L. Minati et al., "Intra- and extra-cranial effects of transient blood pressure changes on brain near-infrared spectroscopy (NIRS) measurements," *J. Neurosci. Methods* **197**, 283–288 (2011).
4. D. A. Boas, A. M. Dale, and M. A. Franceschini, "Diffuse optical imaging of brain activation: approaches to optimizing image sensitivity, resolution, and accuracy," *Neuroimage* **23**(Suppl 1), S275–S288 (2004).
5. R. B. Saager, N. L. Telleri, and A. J. Berger, "Two-detector corrected near infrared spectroscopy (C-NIRS) detects hemodynamic activation responses more robustly than single-detector NIRS," *Neuroimage* **55**, 1679–1685 (2011).
6. T. Yamada, S. Umeyama, and K. Matsuda, "Multidistance probe arrangement to eliminate artifacts in functional near-infrared spectroscopy," *J. Biomed. Opt.* **14**, 064034 (2009).
7. T. Funane et al., "Quantitative evaluation of deep and shallow tissue layers' contribution to fNIRS signal using multi-distance optodes and independent component analysis," *Neuroimage* **85**, 150–165 (2014).
8. G. E. Strangman, Q. Zhang, and Z. Li, "Scalp and skull influence on near infrared photon propagation in the Colin27 brain template," *Neuroimage* **85**, 136–149 (2014).
9. T. Funane et al., "Dynamic phantom with two stage-driven absorbers for mimicking hemoglobin changes in superficial and deep tissues," *J. Biomed. Opt.* **17**, 047001 (2012).